ISSN 0030-400X, Optics and Spectroscopy, 2016, Vol. 120, No. 1, pp. 20–27. © Pleiades Publishing, Ltd., 2016.
Original Russian Text © E.A. Genina, A.N. Bashkatov, M.D. Kozintseva, V.V. Tuchin, 2016, published in Optika i Spektroskopiya, 2016, Vol. 120, No. 1, pp. 27–35.

OPTICS AND SPECTROSCOPY IN BIOPHYSICS AND MEDICINE

OCT Study of Optical Clearing of Muscle Tissue in vitro with 40% Glucose Solution

E. A. Genina[a, b], A. N. Bashkatov[a, b], M. D. Kozintseva[a], and V. V. Tuchin[a, b, c]

[a] *Chernyshevskii Saratov State University, Saratov, 410012 Russia*

[b] *Tomsk State University, Tomsk, 634050 Russia*

[c] *Institute of Precision Mechanics and Control, Russian Academy of Sciences, Saratov, 410028 Russia*

e-mail: eagenina@yandex.ru

Received July 10, 2015

Abstract—The technique of "optical clearing of biological tissues" is aimed at improving the quality of visualization of structures hidden deep in tissue. In this study, we measured the diffusion coefficient of glucose in bovine skeletal muscle tissue by optical coherence tomography (OCT) in vitro and determined changes that took place in the imaging contrast of muscle fibers, the optical depth of coherent probing, and detection under the influence of aqueous 40% solution of glucose. It was shown that, within 90 min, when the depth of coherent probing increased by 14%, the contrast of OCT images increased fourfold and the depth of coherent detection of structural elements of the tissue increased by 2.4 times. The diffusion coefficient of glucose in the muscle tissue was $(2.98 \pm 0.94) \times 10^{-6}$ cm^2/s.

DOI: 10.1134/S0030400X16010082

INTRODUCTION

In recent years, interest in the development and application of optical methods for diagnosing various diseases has been steadily increasing [1–3]. This interest is due to the unique informativeness and relative simplicity, safety, and inexpensiveness of optical devices as compared, for example, to X-ray computed tomography or magnetic resonance imaging (MRI).

One promising optical diagnostic method is optical coherence tomography (OCT). In contrast to other methods such as multiphoton fluorescence [4] and nonlinear microscopy based on second harmonic generation [5], OCT is a simple and accessible method that makes it possible to study the internal microstructure of nontransparent biological tissues to a depth of 3 mm with a spatial resolution of 5–20 μm without destroying their integrity [6, 7].

It is well known that the main limitation of optical diagnostic methods, including OCT, is strong light scattering in biological tissues, which decreases the contrast and spatial resolution and results in a small probing depth [3, 8]. A simple and effective method that allows increasing the probing depth and image quality of interstitial structures is temporary reduction in light scattering in biological tissues using optical clearing agents (OCAs) [8–14].

Optical immersion clearing is based on the impregnation (immersion) of tissue in a biocompatible chemical agent with a relatively high refractive index and hyperosmotic properties. When such agents penetrate into a biological tissue and interact with its components, they facilitate the concordance of refractive indices of scatterers and their environment and temporary changes in the relative position of the structural tissue elements (their ordering) [8]. Aqueous solutions of glycerol, propylene glycol, polyethylene glycol, etc., are used as OCAs [8–14]. Along with the specified immersion agents, aqueous solutions of glucose are widely used [15].

The study of the kinetics of changes in the scattering properties of biological tissue after the penetration of OCA made it possible to develop a procedure for assessing the permeability of various tissues using OCT [12, 16–19]. In turn, the monitoring of diffusion of OCAs with a high resolution in time and depth makes it possible to differentiate between healthy and pathologically altered biological tissues [20–24]. Earlier, optical clearing of muscle tissue by OCAs was studied in [25–32] using integrating sphere spectroscopy, as well as confocal and nonlinear microscopy. In these studies, samples of abdominal-wall muscle tissue and skeletal muscles of rodents and porcine myocardium were analyzed. Diffusion coefficients of glucose in the abdominal muscle and myocardium were measured in [31, 32]. However, despite the similarity of different types of muscle tissue, the diffusion coefficients in them significantly differ, which is apparently due to the differences in the structure and component composition of these tissues.

Thus, the purpose of this study was to measure the diffusion coefficient of glucose in the skeletal muscle

and to estimate the changes in contrast and depth of imaging of muscle fibers using OCT, which can be used for the development of methods for diagnosing pathological changes in the muscle tissue.

MATERIALS AND METHODS

The study was performed with eight samples of bovine muscle tissue in vitro. Before starting the experiment, the biological tissue was cut into samples (approximately 20 × 15 mm), with the fibers arranged in parallel to the surface. The thickness of the samples was measured with a micrometer with an accuracy of ±10 μm in several points and then averaged. The average value of the thickness of the studied samples before and after clearing was 1.9 ± 0.18 and 2.63 ± 0.54 mm, respectively.

A 40% glucose solution (solution for intravenous administration, Novosibkhimpharm, Russia) was used as an OCA. The refractive index of the solution, measured with a DR-M2/1550 refractometer (Atago, Japan) at a wavelength of 930 nm, was 1.37; the pH of the solution, measured with a pH meter (Hanna, Germany), was ~3.5.

The optical clearing of the biological tissue was studied using an OCP930SR 022 spectral optical coherence tomography (Thorlabs, United States) with an operating wavelength of 930 ± 5 nm and a bandwidth at half maximum of the emission peak of 100 ± 5 nm. The optical power of the probing light was 2 mW, and the scanned area was 6 mm. The axial and lateral resolutions of the instrument on air were 6.2 and 9.6 μm, respectively. Muscle tissue samples were placed in a specially designed cell with an opening in the top wall, through which the cell was then filled with a glucose solution. Each area was scanned before the addition of the glucose solution and during optical clearing for 90 min. B-scans were recorded every 2–5 min.

The complete light attenuation coefficient in the biological tissue area μ_t (the sum of absorption coefficient μ_a and scattering coefficient μ_s) can be obtained by selecting the parameters of the approximating curve calculated using an appropriate model in the area of interest in the slope of A-scan of the OCT signal [6, 33, 34].

A single scattering model is based on the assumption that only the light that experienced single scattering retains the coherence properties and contributes to the formation of the OCT signal. The single scattering model is valid for both weakly scattering biological tissues and for the surface layers of biological tissue, where the single backscattering mode is predominant [34]. The OCT signal in this case is defined as [6, 33, 34]

$$\left(\left\langle i^2(z)\right\rangle\right)^{1/2} \approx \left(\left\langle i^2\right\rangle_0\right)^{1/2} \left(\exp(-2\mu_t z)\right)^{1/2}, \qquad (1)$$

where $i(z)$ is an OCT signal and z is the distance from the tissue surface to the area from which the reflected signal came.

It is known that the result of an OCT study is the measurement of the dependence of the OCT signal intensity of the studied tissue, $R(z) \propto (\langle i^2(z)\rangle)^{1/2}$, on depth z. The OCT signal intensity depends on reflectivity $\alpha(z)$ of biological tissue at a given depth, determined by the local refractive index and local ability of biological tissue to backscatter light, and the complete attenuation coefficient $\mu_t = \mu_a + \mu_s$ of biological tissue. According to the single scattering model, the reflected power is proportional to $\exp(-\mu_t z)$ [6], i.e., can be approximated by equation

$$R(z) = A\exp(-\mu_t z) + B, \qquad (2)$$

where A is the proportionality coefficient equal to $P_0\alpha(z)$, P_0 is the optical power of the beam incident on the surface of the biological tissue, and B is the background signal.

Figure 1 shows the average A-scan of the OCT signal from the muscle tissue and the approximating curve constructed using the single scattering model. For the analysis, an area of 51 A-scans in width (approximately 150 μm) was selected on the B-scan. The selection of coefficients in Eq. (2) for approximating the experimental curve allows estimating the depth-average (efficient) coefficient of light attenuation by the muscle tissue.

Structurally, the skeletal muscle studied in this work is classified as a kind of striated muscle tissue. It consists of numerous elongated filaments. A muscle fiber is considered to be a multinucleated cell covered with sarcolemma (~10-nm membrane). The diameter of a functionally mature striated muscle fiber usually

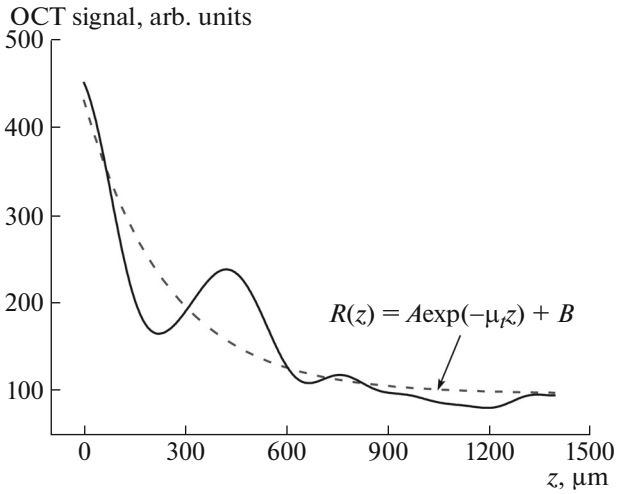

Fig. 1. Averaged A-scan of the OCT signal from bovine muscle tissue (solid line) and the approximating curve constructed using the single scattering model (dashed line).

varies from 10 to 100 μm, and the fiber length corresponds to the length of the muscle. The sarcoplasm of each muscle fiber contains numerous longitudinal filamentary structures, myofibrils, packed in bundles and surrounded with the cell membrane. The thickness of a myofibril is less than 1 μm [35]. The sarcoplasm of muscle fibers also contains a number of other structures including mitochondria, the volume fraction of which, according to various data, is ~5% [36] or varies from 4 to 15% [37] of the fiber volume.

The muscle tissue of adult animals and humans contains from 72 to 80% of water. Approximately 20–28% of the muscle weight is the dry residue (primarily proteins). The major proteins of muscle fibers are myosin (50–55% of the dry weight of myofibrils) and actin (20% of the dry weight of myofibrils). Thick filaments (myofilaments) are formed as a result of joining a large number of myosin molecules spatially oriented in a certain way. In addition to proteins, the dry residue contains glycogen and other carbohydrates, lipids, and various other chemical compounds [35].

According to the published data, the refractive index of bovine skeletal muscles, measured in the range of 560–640 nm, is 1.382 ± 0.004 [38]. Assuming that the volume fraction of muscle fibers is 0.244 ± 0.003 [39] and the mean refractive index of interstitial fluid is 1.35 [40], the refractive index of muscle fibers can be estimated as 1.481 using the Gladstone–Dale law [3], which agrees well with the values of 1.46 and 1.53 reported in [39, 40]. Muscle fibers, in turn, are formed from protein myofibrils and mitochondria. Since the refractive index of mitochondria is 1.4 [41], the refractive index of the myosin–actin fibers can be estimated as 1.49 ± 0.005. Thus, a simplified model of a skeletal muscle represents a system of densely packed cylinders with a refractive index of 1.49, arranged in parallel to each other in the interstitial fluid (a mixture of extracellular and intracellular fluids), the volume fraction of which is 0.21–0.23, and spherical scatterers approximately 0.5 ± 0.1 μm in diameter [42] with a refractive index of 1.4, the volume fraction of which is approximately 0.02–0.04.

Since muscle fibers are arranged in parallel to the surface, the diffusion of OCAs into the tissue and water from the tissue proceeds through the membrane of muscle-fiber bundles and the sarcolemma; however, in this model, the rate of diffusion in these membranes and in cytoplasm layers is not considered separately. Diffusion is averaged over the entire volume of biological tissue. Thus, the diffusion of a glucose solution in the muscle tissue can be described within the framework of the free diffusion theory with certain assumptions concerning the transfer process: that (1) the exchange flux of glucose molecules into the biological tissue and water from it at a given point is proportional to the glucose concentration gradient at this point, (2) the diffusion coefficient is constant at all points inside the test sample, and (3) two-way diffusion into the muscle tissue takes place.

The geometric pattern can be represented as a plane-parallel plate of a finite thickness. Since the area of the upper and lower surfaces of the plate is much larger than the area of its lateral sides, the edge effects can be neglected. Therefore, it is possible to solve a one-dimensional diffusion problem:

$$\frac{\partial C(x,t)}{\partial t} = D\frac{\partial^2 C(x,t)}{\partial^2 x}, \tag{3}$$

where $C(x, t)$ is the glucose concentration in the muscle tissue sample (g/mL), D is the diffusion coefficient (cm^2/s), x is the spatial coordinate in the thickness of biological tissue sample (cm), and t is the duration of diffusion of the solution into the tissue (s). In the first approximation, the solution of this equation takes the form [43]

$$C(t) = C_0\left(1 - \exp\left(-t\pi^2\frac{D}{l^2}\right)\right). \tag{4}$$

An optical model of muscle tissue represents a system of densely packed thin dielectric cylinders, which are arranged in parallel to each other, and balls, which are uniformly distributed in the space between the cylinders. The scattering coefficient of muscle tissue μ_s can be written as [44, 45]

$$\mu_s = \frac{\varphi_1}{\pi a_1^2}\sigma_{s1}(m,x)\frac{(1-\varphi_1)^3}{(1+\varphi_1)} + \frac{\varphi_2}{\frac{4}{3}\pi a_2^3}\sigma_{s2}(m,x)\frac{(1-\varphi_2)^4}{(1+2\varphi_2)^2}, \tag{5}$$

where φ_1 is the volume fraction of the cylindrical scatterers in the muscle tissue, φ_2 is the volume fraction of the spherical scatterers in the muscle tissue, a_1 is the radius of cylinders, a_2 is the radius of the spherical scatterers, $\sigma_{s1}(m,x)$ is the scattering cross-section of the cylindrical scatterers, $\sigma_{s2}(m,x)$ is the scattering cross-section of the spherical scatterers, $m = n_s/n_I$ is the relative refractive index of scatterers, $x = 2\pi a n_I/\lambda$ is the diffraction parameter, $n_I = n_{I0}(1 - C) + n_s C$, n_I is the refractive index of the interstitial fluid, nI_0 is the refractive index of the interstitial fluid at the initial time, n_s is the refractive index of muscle fibers or mitochondria in the sample, and C is the concentration of glucose in the muscle tissue.

Equation (5) defines the dependence of the scattering coefficient on the glucose concentration in the muscle tissue sample (i.e., forms the direct problem). The inverse problem in this case is the reconstitution of the diffusion coefficient value by the time depen-

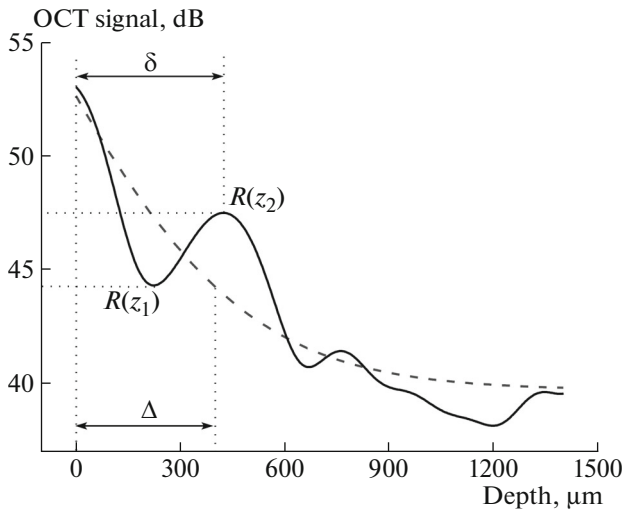

Fig. 2. Method for determination of contrast $|R(z_1) - R(z_2)|/[R(z_1) + R(z_2)]$, coherent probing depth Δ, and coherent detection depth δ based on analysis of the signal intensity distribution on an OCT image.

dence of the scattering coefficient. This problem is solved by minimizing the target function

$$f(D) = \sum_{i=1}^{N} (\mu_s(D,t_i) - \mu_s^*(t_i))^2, \quad (6)$$

where N is the total number of experimental points obtained when recording the dynamics at a fixed wavelength, $\mu_s(D,t_i)$ is the scattering coefficient calculated by formula (5) at time t for a given value D, and $\mu_s^*(t_i)$ is the experimentally measured value of the coefficient scattering at time t [43].

To minimize the target function, we used the integrated method described in detail in [46]. The iterative procedure was repeated until matching the experimental and calculated data.

During the optical clearing of the muscle tissue we determined the contrast of OCT images, the coherent probing depth (CPD) [47], and the coherent detection depth (CDD) [48] (Fig. 2). The contrast of the obtained images was estimated by the formula

$$\text{Contrast} = \frac{|R(z_1) - R(z_2)|}{R(z_1) + R(z_2)}, \quad (7)$$

where $R(z_1)$ and $R(z_2)$ are the minimum and maximum, respectively, amplitudes of the averaged OCT signal obtained from the muscle tissue image. The contrast values were calculated at optical depths of ~350–360 and ~785–790 μm, corresponding to individual depths of muscle fibers.

The CPD Δ was determined by the level corresponding to reduction of the curve approximating the OCT signal by e times. The CDD of the object within the tissue δ was defined as the distance between the peaks of intensity of the signal from the sample surface and the useful signal from the depth of the tissue. In this case, the deepest layer of muscle tissue, which was visualized on the OCT image, served as a detection object (Figs. 3a, 3f). Contrast values Δ and δ were determined in several areas of the OCT image averaged over ten A-scans. The results from different areas were also averaged, and the standard deviation was calculated.

RESULTS AND DISCUSSION

Figure 3 shows the OCT images of the muscle tissue before the optical clearing and at different time intervals after its beginning. The layered structure of the tissue can be well seen (numbers in Figs. 1a and 1f indicate the visualized layers). The bars and letter δ indicate the CDD of the biological tissue.

Figure 4 shows the distribution of the OCT signal averaged over the depth for the images shown in Figs. 3a, 3c, and 3f. Maxima on the curves correspond to the light areas on the OCT images characterizing the muscle tissue layers, and minima correspond to the boundaries between the layers. It can also be seen that deeper layers are visualized better over time: the third layer is not visible in the intact sample, whereas it is seen quite clearly 20 min after the start of immersion. After 90 min, the second and third layers become even more visible.

Figure 5 shows the results of calculating the contrast of OCT images of the second and third layers of the muscle tissue lying at optical depths of ~785–790 and ~350–360 μm. The contrast of the second layer increased by almost four times, from 0.026 ± 0.004 to 0.099 ± 0.005, and the contrast of the third layer increased from zero to 0.027 ± 0.003.

The CPD of the intact muscle tissue, as assessed by OCT imaging, was 350 ± 20 μm. For the intact tissue, CPD and CDD values practically coincided. However, 90 min after the beginning of exposure to the glucose solution, the CPD of the biological tissue increased to an average of 400 ± 30 μm (approximately by 14%). The CDD value increased from 350 ± 15 to 830 ± 20 μm (i.e., approximately by 2.4 times).

In [49], the depth of detection of the considered tissue (intact sample of lumbar intervertebral disc, ~600 μm) was much greater than the CDD of an intact sample of bovine skeletal muscle obtained in this present study (~350 μm). Apparently, the differences in the depth of the useful signal obtained from OCT images are due, first, to the differences in the structure and properties of the studied tissues and, second, with the polarization OCT technique used by the authors of [49], which makes it possible to improve the image of tissues with strong anisotropic properties.

The results of calculations of the diffusion coefficient of glucose in the muscle tissue for each of the

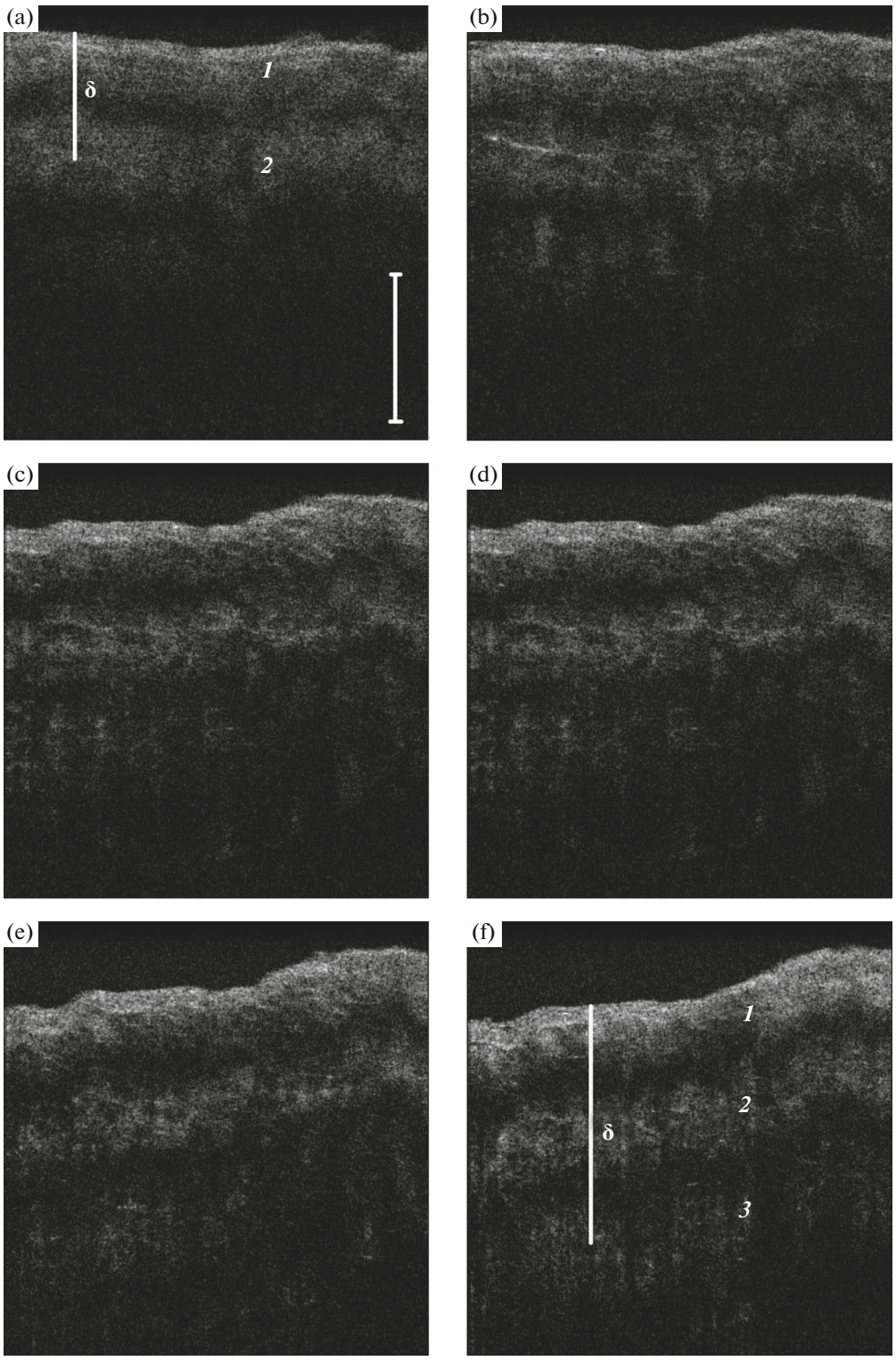

Fig. 3. OCT images of bovine muscle tissue (a) before optical clearing and (b) 10, (c) 20, (d) 30, (e) 60, and (f) 90 min after its immersion in a 40% aqueous solution of glucose. Scale bar—0.5 mm. The segment and letter δ indicate the coherent detection depth. The numbers indicate the visualized layers of the biological tissue.

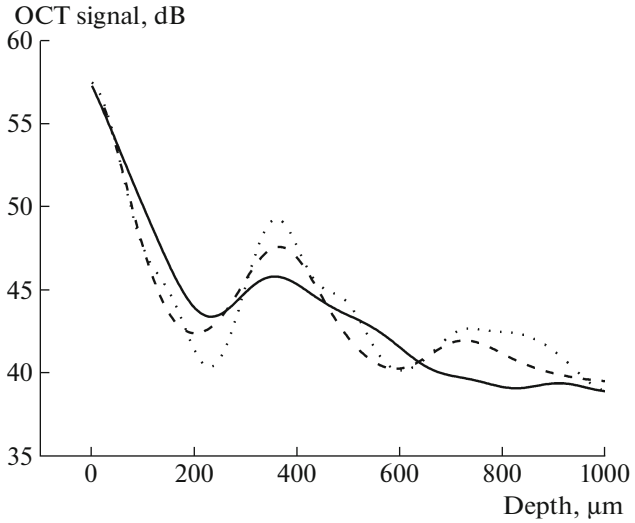

Fig. 4. Distribution of the OCT signal averaged over the depth for the images shown in Figs. 3a, 3c, and 3f before clearing (solid line) and 20 min (dashed line) and 90 min (dotted line) after the beginning of clearing.

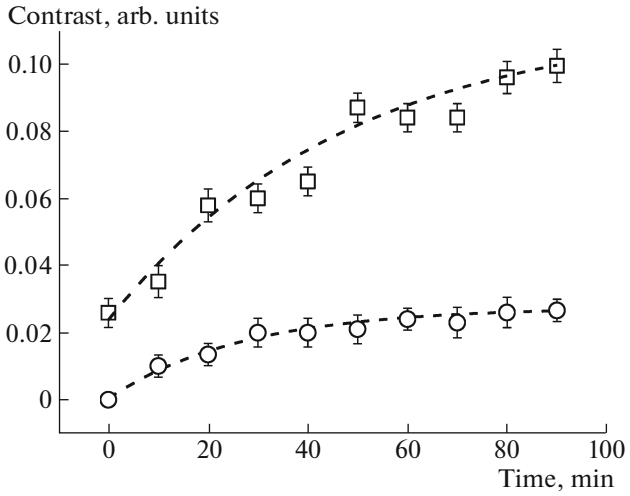

Fig. 5. Dynamics of changes in the contrast of OCT images of bovine muscle tissue at optical depths of ~355–360 (□) and ~785–790 (○) μm. Vertical bars represent the standard deviation.

eight samples are summarized in the table. The mean value of the diffusion coefficient was $(2.98 \pm 0.94) \times 10^{-6}$ cm^2/s.

The difference between the refractive indices of interstitial fluid (1.35), myofilaments (1.49), and mitochondria (1.4) causes a strong scattering of biological tissue. Under the influence of glucose, which penetrates into the interstitial space, the refractive indices of the components of the biological tissue are concerted, which leads to an increase in its optical transparency. For example, the authors of [31] showed that, under the influence of 40% glucose solution, the collimated transmission coefficient of a rat abdominal muscle sample increased by more than 70% within 30 min at a wavelength of 900 nm. According to [32], the collimated transmission coefficient of porcine myocardium increased by approximately five times for 85 min at a wavelength of 900 nm when a 40% glucose solution was used as an OCA.

The authors of [16] determined the permeability coefficient of the sclera for a glucose solution depending on depth. They showed that the rate of glucose diffusion into the sclera was nonlinear, increasing upon the transition from the surface epithelial layer to the stroma. In contrast to [16], we estimated the effective diffusion coefficient, which was averaged over the probing depth. Since the skeletal muscle has a complex layered structure, the dependence of the diffusion coefficient of glucose on depth can also be nonlinear, and the estimation of the diffusion coefficient in the individual layers of muscle tissue lying at different depths to test this hypothesis is a promising task for further studies.

The authors of [31, 32] also calculated the diffusion coefficients of glucose averaged for the entire sample in different types of muscle tissue. The coefficient of glucose diffusion into the abdominal muscle, according to [31], was 8.3×10^{-7} cm^2/s. The diffusion coefficient of a similar solution in the myocardium, determined in [32], was 4.75×10^{-7} cm^2/s. These values differ from our data ($(2.98 \pm 0.94) \times 10^{-6}$ cm^2/s). These differences, in our opinion, may be due primarily to the differences in the measurement and calculation methods and, probably, the differences in the structural and chemical properties of the samples them-

Diffusion coefficient of glucose in bovine muscle tissue in vitro

Sample	Thickness, mm	Diffusion coefficient, cm^2/s	Sample	Thickness, mm	Diffusion coefficient, cm^2/s
1	1.77	2.44×10^{-6}	5	1.93	2.48×10^{-6}
2	2.17	4.99×10^{-6}	6	1.78	2.54×10^{-6}
3	1.93	3.83×10^{-6}	7	1.95	2.51×10^{-6}
4	1.88	2.48×10^{-6}	8	1.50	2.57×10^{-6}

Mean value of diffusion coefficient $\langle D \rangle = (2.98 \pm 0.94) \times 10^{-6}$ cm^2/s.

selves, because they were taken from different animals and different organs, and the sample preparation methods. For example, the density of myocardium is approximately 1.057 g/cm^3 [40] and the density of the abdominal muscle is approximately 1.05 g/cm^3 [50], whereas the density of the bovine muscle tissue, used in this study, is 0.937–0.953 g/cm^3 [51]. It is obvious that the smaller density of muscle tissue is determined by the high content of free water in it and, therefore, the bovine muscle tissue, studied in this work, should have the highest permeability. Thus, the diffusion coefficient of glucose in it is greater than in the muscle tissue of other types.

The differences in the diffusion rates may be related to the differences in the pH values of the solutions used. To analyze the effect of pH, we prepared a 40% aqueous solution of glucose similarly to the procedure used in [31]. The measured pH value of this solution was 5.59. The authors of [31] reported a slight dehydration of biological tissue samples as a result of optical clearing. However, the use in this study of the 40% glucose solution for intravenous administration, which is more acidic (pH ~ 3.5), conversely, caused a significant increase in the thickness of the biological tissue sample (on average by ~38%). This phenomenon can be explained by the shift in the pH value of the interstitial fluid from the isoelectric point of proteins and respective swelling of the biological tissue [52]. Apparently, an increase in the tissue volume as a result of swelling leads to the loosening of fibers and an increase in the interstitial space, which, in turn, accelerates diffusion, whereas the dehydration of tissue (i.e., an increase in its density) hampers the penetration of OCA molecules into the interstitial space. However, in [32], the use of the same glucose solution for intravenous administration (pH ~3.5) for optical clearing of the myocardial tissue caused a decrease in the thickness of samples by an average of 14%. In our opinion, this inconsistency was due to the differences in the protein composition of skeletal and cardiac muscles. For example, the content of myofibrillar proteins in the myocardium is much lower (~40% of the fiber volume) compared to the skeletal muscle (~70% of the fiber volume) [35, 53], whereas the concentration of stromal proteins in the myocardium is higher than in the skeletal muscle [35]. Apparently, these structural characteristics and chemical composition of the myocardium prevent its swelling in solutions with low pH.

CONCLUSIONS

The optical clearing of bovine skeletal muscle tissue in vitro with a 40% glucose solution resulted in a fourfold increase in the image contrast of objects located at a depth of ~360 μm and a significant increase in the image contrast at a depth of more than 800 μm from the surface of the biological tissue, which led to an ~2.4-fold increase in the coherent detection depth in OCT. The diffusion coefficient of glucose in the muscle tissue was measured. The results can be used in the development of procedures for optical clearing of muscle tissue in vivo.

ACKNOWLEDGMENTS

This study was supported by the Mendeleev Foundation of Tomsk State University and supported in part by the program of the President of the Russian Federation "Leading Scientific Schools," project no. NSh-703.2014.2.

REFERENCES

1. *Handbook of Optical Biomedical Diagnostics,* Ed. by V. V. Tuchin, SPIE Press Monographs, Vol. 107 (Bellingham, SPIE Press, 2002).
2. *Biomedical Photonics Handbook,* Ed. by T. Vo-Dinh (CRC Press, Boca Raton, 2003).
3. V. V. Tuchin, *Tissue Optics: Light Scattering Methods and Instruments for Medical Diagnosis,* SPIE Press Monograph, Vol. 166 (Fizmatlit, Moscow, 2012; SPIE Publ., 2007).
4. P. T. C. So, C. Y. Dong, and B. R. Masters, in *Biomedical Photonics Handbook,* Ed. by T. Vo-Dinh (CRC, Boca Raton, FL, 2003).
5. *Second Harmonic Generation Imaging,* Ed. by F. S. Pavone and P. J. Campagnola (Taylor and Francis Group, CRC Press, Boca Raton, 2014).
6. R. K. Wang and V. V. Tuchin, in *Handbook of Coherent-Domain Optical Methods. Biomedical Diagnostics, Environmental Monitoring, and Material Science,* 2nd ed., Ed. by V. V. Tuchin (Springer, New York, Heidelberg, Dordrecht, London, 2013), Vol. 2.
7. N. D. Gladkova, N. M. Shakhova, and A. M. Sergeeva, *Practical Guide on Optical Coheren Tomography* (Fizmatlit, Moscow, 2007) [in Russian].
8. V. V. Tuchin, *Optical Clearing of Tissues and Blood,* SPIE Press Monograph, Vol. 154 (SPIE Press, Belligham, 2006).
9. S. G. Proskurin and I. V. Meglinski, Laser Phys. Lett. **4**, 824 (2007).
10. Y. M. Liew, R. A. McLaughlin, F. M. Wood, and D. D. Sampson, J. Biomed. Opt. **16**, 116018 (2011).
11. E. A. Genina, A. N. Bashkatov, and V. V. Tuchin, Expert Rev. Med. Dev. **7**, 825 (2010).
12. K. V. Larin, M. G. Ghosn, A. N. Bashkatov, E. A. Genina, N. A. Trunina, and V. V. Tuchin, IEEE J. Sel. Top. Quantum Electron. **18**, 1244 (2012).
13. X. Wen, S. L. Jacques, V. V. Tuchin, and D. Zhu, J. Biomed. Opt. **17**, 066022 (2012).
14. E. A. Genina, A. N. Bashkatov, Yu. P. Sinichkin, I. Yu. Yanina, and V. V. Tuchin, J. Biomed. Photon. Eng. **1**, 22 (2015).
15. E. A. Genina, A. N. Bashkatov, and V. V. Tuchin, in *Handbook of Optical Sensing of Glucose in Biological Fluids and Tissues,* Ed. by V. V. Tuchin (Taylor Francis Group, CRC Press, Boca Raton, 2009), p. 657.

16. M. G. Ghosn, V. V. Tuchin, and K. V. Larin, Opt. Lett. **31**, 2314 (2006).
17. M. G. Ghosn, N. Sudheendran, M. Wendt, A. Glasser, V. V. Tuchin, and K. V. Larin, J. Biophoton. **3**, 25 (2010).
18. E. A. Genina, A. N. Bashkatov, K. V. Larin, T. G. Kamenskikh, and V. V. Tuchin, Quantum Electron. **41**, 407 (2011).
19. X. Guo, G. Wu, H. Wei, X. Deng, H. Yang, Y. Ji, Y. He, Z. Guo, S. Xie, H. Zhong, Q. Zhao, and Z. Zhu, Photochem. Photobiol. **88**, 311 (2012).
20. M. G. Ghosn, E. F. Carbajal, N. A. Befrui, A. Tellez, J. F. Granada, and K. V. Larin, J. Biomed. Opt. **13**, 010505 (2008).
21. H. Q. Zhong, Z. Y. Guo, H. J. Wei, C. C. Zeng, H. L. Xiong, Y. H. He, and S. H. Liu, Laser Phys. Lett. **7**, 315 (2010).
22. Q. L. Zhao, J. L. Si, Z. Y. Guo, H. J. Wei, H. Q. Yang, G. Y. Wu, S. S. Xie, X. Y. Li, X. Guo, H. Q. Zhong, and L. Q. Li, Laser Phys. Lett. **8**, 71 (2011).
23. Z. Zhu, G. Wu, H. Wei, H. Yang, Y. He, S. Xie, Q. Zhao, and X. Guo, J. Biophoton. **5**, 1 (2012).
24. D. K. Tuchina, R. Shi, A. N. Bashkatov, E. A. Genina, D. Zhu, Q. Luo, and V. V. Tuchin, J. Biophoton. **8**, 332 (2015).
25. R. Dickie, R. M. Bachoo, M. A. Rupnick, S. M. Dallabrida, G. M. de Loid, J. Lai, R. A. de Pinho, and R. A. Rogers, Microvasc. Res. **72**, 20 (2006).
26. S. Plotnikov, V. Juneja, A. B. Isaacson, W. A. Mohler, and P. J. Campagnola, Biophys. J. **90**, 328 (2006).
27. O. Nadiarnykh and P. J. Campagnola, Opt. Express **17**, 5794 (2009).
28. R. LaComb, O. Nadiarnykh, S. Carey, and P. J. Campagnola, J. Biomed. Opt. **13**, 021109 (2008).
29. O. Nadiarnykh and P. J. Campagnola, in *Second Harmonic Generation Imaging,* Ed. by F. S. Pavone and P. J. Campagnola (Taylor and Francis Group, CRC Press, Boca Raton, London, New York, 2014), pp. 169–189.
30. L. M. Oliveira, M. I. Carvalho, E. Nogueira, and V. V. Tuchin, Laser Phys. **23**, 075606 (2013).
31. L. Oliveira, M. I. Carvalho, E. Nogueira, and V. V. Tuchin, J. Innovative Opt. Health Sci. **6**, 1350012 (2013).
32. D. K. Tuchina, A. N. Bashkatov, E. A. Genina, and V. V. Tuchin, J. Innovative Opt. Health Sci. **8**, 1541006 (2015).
33. D. J. Faber, F. J. van der Meer, M. C. G. Aalders, and T. G. van Leeuwen, Opt. Express **12**, 4353 (2004).
34. P. Lee, W. Gao, and X. Zhang, Appl. Opt. **49**, 3538 (2010).
35. T. T. Berezov and B. F. Korovkin, *Biological Chemistry* (Meditsina, Moscow, 1998) [in Russian].
36. S. Schiaffino and C. Reggiani, Physiol. Rev. **91**, 1447 (2011).
37. S. Larsen, J. Nielsen, C. N. Hansen, L. B. Nielsen, F. Wibrand, N. Stride, H. D. Schroder, R. Boushel, J. W. Helge, F. Dela, and M. Hey-Mogensen, J. Physiol. **590**, 3349 (2012).
38. J. J. J. Dirckx, L. S. Kuypers, and W. F. Decraemer, J. Biomed. Opt. **10**, 044014 (2005).
39. L. Oliveira, A. Lage, M. Pais Clemente, and V. V. Tuchin, Opt. Lasers Eng. **47**, 667 (2009).
40. R. C. Haskell, F. D. Carlson, and P. S. Blank, Biophys. J. **56**, 401 (1989).
41. R. Thar and M. Kuhl, J. Theor. Biol. **230**, 261 (2004).
42. J. R. Mourant, J. P. Freyer, A. H. Hielscher, A. A. Eick, D. Shen, and T. M. Johnson, Appl. Opt. **37**, 3586 (1998).
43. A. N. Bashkatov, E. A. Genina, and V. V. Tuchin, in *Handbook of Optical Sensing of Glucose in Biological Fluids and Tissues,* Ed. by V. V. Tuchin (Taylor & Francis Group LLC, CRC Press, Boca Raton, 2009), pp. 587–621.
44. C. Bohren and D. Huffman, *Absorption and Scattering of Light by Small Particles* (Wiley, New York, 1983).
45. J. M. Schmitt and G. Kumar, Appl. Opt. **37**, 2788 (1998).
46. B. D. Bunday, *Basic Optimization Methods* (Arnold, London, 1984).
47. S. G. Proskurin, Quantum Electron. **42**, 495 (2012).
48. E. A. Genina, G. S. Terentyuk, B. N. Khlebtsov, A. N. Bashkatov, and V. V. Tuchin, Quantum Electron. **42**, 478 (2012).
49. N. Ignatieva, I. Andreeva, V. Lunin, O. Zakharkina, E. Sobol, and V. Kamensky, Lasers Surg. Med. **40**, 422 (2008).
50. W. Schneider, T. Bortfeld, and W. Schlegel, Phys. Med. Biol. **45**, 459 (2000).
51. Veterinary medicine for all. Meat features of different species of animals, birds and wildfowl with fat constants. http://vetfac.narod.ru/otlichija0mjasa.htm. Cited July 1, 2015.
52. A. V. Lykov, *Transport Phenomena in Capillary-Porous Bodies* (Gos. Izdat. Tekh.-Teor. Liter., Moscow, 1954) [in Russian].
53. S. L. Kuznetsov, N. N. Mushkambarov, and V. L. Goryachkina, Guide-Atlas of Histology, Cytology and Embryology. http://nsau.edu.ru/images/vetfac/images/ebooks/histology/histology/r4/t11.html. Cited July 1, 2015.

Translated by M. Batrukova